



Research Article

The Accumulation Characteristics of the Paleozoic Reservoir in the Central-Southern Ordos Basin Recorded by Organic Inclusions

Ruijing Zhu ^{1,2}, Rongxi Li ¹, Xiaoli Wu,¹ Xiaoli Qin,¹ Bangsheng Zhao,¹ Futian Liu,¹ and Di Zhao¹

¹School of Earth Science and Resources, Chang'an University, Xi'an, Shaanxi 710054, China

²Shanxi Institute of Engineering Technology, Yangquan, Shanxi 045000, China

Correspondence should be addressed to Rongxi Li; rongxi99@163.com

Received 22 May 2021; Revised 22 July 2021; Accepted 24 August 2021; Published 16 September 2021

Academic Editor: Giovanni Mongelli

Copyright © 2021 Ruijing Zhu et al. This is an open access article distributed under the Creative Commons Attribution License, which permits unrestricted use, distribution, and reproduction in any medium, provided the original work is properly cited.

The Permian tight clastic reservoir and Ordovician carbonate reservoir were developed in the central-southern Ordos Basin. This study investigated the fluid inclusion petrography, diagenetic fluid characteristics, formation process of natural gas reservoir, source rock characteristics, and reservoir accumulation characteristics of these Paleozoic strata by petrographic observations, scanning electron microscope imaging, fluid inclusion homogenization temperature, salinity, laser Raman spectrum, and gas chromatograph analyses. The results have suggested two phases of fluid inclusions in both the Permian sandstone and the Ordovician Majiagou Formation dolomite reservoirs, and the fluid inclusions recorded the history from the early thermal evolution of hydrocarbon generation to the formation, migration, and accumulation of natural gas. The early-phase inclusions show weak yellow fluorescence and recorded the early formation of liquid hydrocarbons, while the late-phase inclusions are nonfluorescent natural gas inclusions distributed in the late tectonic fractures and recorded the late accumulation of natural gas. The brine systems of the Permian and Ordovician fluid inclusions are, respectively, dominated by $\text{CaCl}_2\text{-H}_2\text{O}$ and $\text{MgCl}_2\text{-NaCl-H}_2\text{O}$. The diagenetic fluids were in the ranges of medium-low temperature and moderate-low salinity. The natural gas hydrocarbon source rocks in the Ordos Basin include both the Permian coal-bearing rocks and the Ordovician carbonates. The process of the early-phase liquid hydrocarbon formation and migration into the reservoir corresponded to 220 Ma (Late Triassic). The late large-scale migration and accumulation of natural gas occurred at 100 Ma (early Late Cretaceous), which was close to the inclusion Rb/Sr isochron age of 89.18 Ma, indicating that the natural gas accumulation was related to the Yanshanian tectonic movement.

1. Introduction

The Ordos Basin is one of the most important natural gas resource exploration and development bases in China. At present, most discovered natural gas are stored in the Upper Paleozoic Permian clastic rock reservoir and the Lower Paleozoic Ordovician carbonate reservoir, and their natural gas accumulation theories have been established based on a large number of studies. In the Upper Paleozoic, the extensive hydrocarbon generation and continuous charging of coal source rocks provided high-quality gas source conditions. The large-scale delta distributary channel sand bodies,

spreading from north to south and stacking vertically, comprise the reservoirs. Natural gas migration and accumulation in a close range formed the large tight gas reservoirs [1–3]. The Lower Paleozoic Ordovician natural gas reservoirs are mainly karst cavernous reservoirs and dolomite reservoirs, and the gas accumulation was mainly controlled by karst paleogeomorphology [4–6].

However, both the Permian tight gas reservoirs and the Ordovician carbonate gas reservoirs discovered in the Ordos Basin are mainly distributed in the northern part of the basin, while the exploration progress in the vast southern area is relatively slow. Previous studies on the southern part

of the basin mainly focused on the characteristics and evaluation of hydrocarbon source rocks, the genesis and source of natural gas, clastic rock reservoirs, karst paleogeomorphology, characteristics, accumulation, and evolution of the carbonate reservoirs [7–17]. Some scholars [18–20] believe that the natural gas in the northern part of the Ordos Basin originated from the southern region, and the natural gas migrated and accumulated on a large scale from south to north. The natural gas in the early Paleozoic gathered around the old central uplift in the form of liquid hydrocarbons, which then became gaseous due to thermal cracking. These gaseous hydrocarbons then migrated northeastward from the central uplift and accumulated in the northern reservoirs. Wang [12] proposed three stages of oil and gas filling in the Shanxi Formation of the Lower Paleozoic at the end of Triassic, middle and late Jurassic, and the end of Early Cretaceous, respectively. Wang [13] believed that the “self-generation-self-storage” and the “lower-generation-upper-storage” were the main types of source-reservoir-cap assemblages, and the regional uplift movement around the end of the Early Cretaceous was the key period for the large-scale migration and accumulation of oil and coal gas in this area. Wang et al. [14] argued that the oil generated from the Pingliang Formation hydrocarbon source rocks accumulated in the weathering layer of the Lower Paleozoic at the central paleo-uplift, which was then transformed into a gas reservoir. Despite the abundant studies, many problems still remain unsolved concerning the Paleozoic gas reservoirs in the southern Ordos Basin, such as the diagenetic evolution of reservoirs, gas accumulation phases, and the diagenetic fluid characteristics.

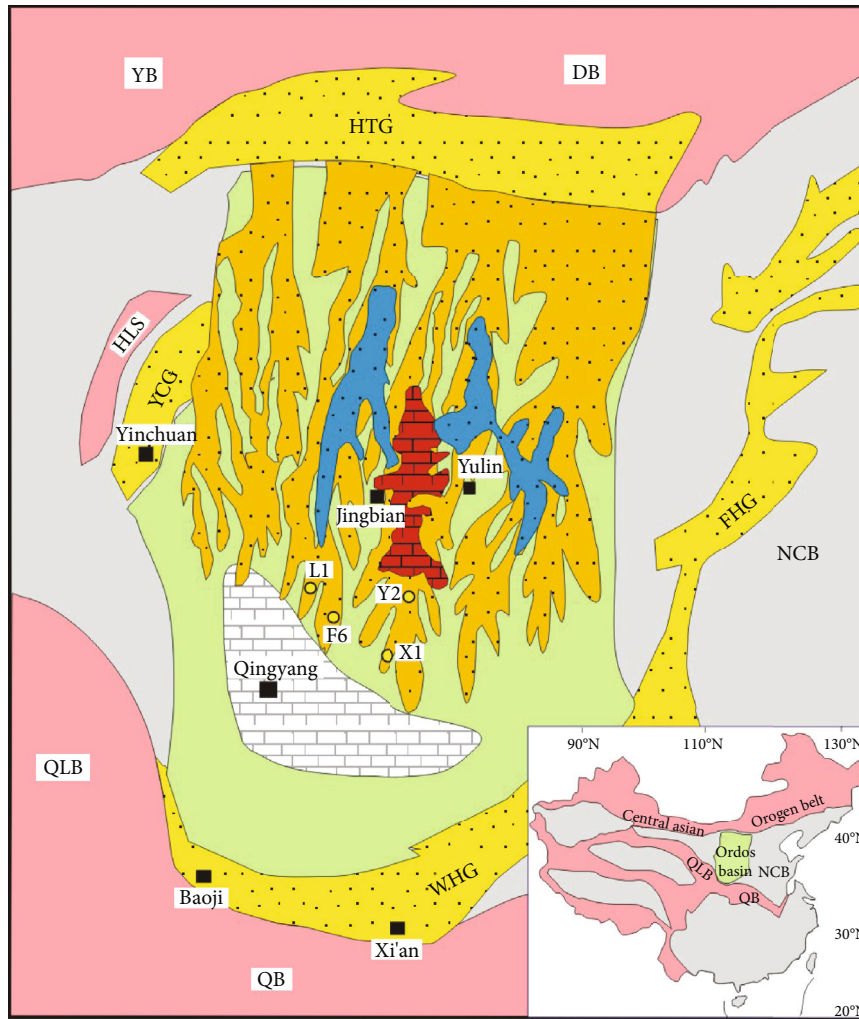
This study investigated core samples from exploration wells by petrographic observation, scanning electron microscope imaging, fluid inclusion homogenization temperature, salinity, laser Raman spectrum, and gas chromatograph analyses. The investigation will not only better characterize the petrography of the fluid inclusions but also reveal the source rock characteristics, diagenetic fluid characteristics, isotopic dating, the natural gas components, gas accumulation characteristics, and phases.

2. Geological Setting

The Ordos Basin is one of the most important fossil-fuel energy basins in west-central China and contains large reserves of coal, oil, natural gas, and coalbed methane [21–23]. It is a large intracontinental, superimposed, and residual basin in the North China block [24–26] and is composed of six subtectonic units, including the Yimeng uplift, Western thrust zone, Tianhuan syncline, Yishan monocline, Jinxi fold belt, and Weibei uplift [27, 28]. The main target strata of this study are the Upper Paleozoic Permian and Lower Paleozoic Ordovician Majiagou Formation. Late Carboniferous and Permian strata experienced a transition from an epeiric sea to an inland lake basin. Sediments were mainly developed in shallow shelves, shallow deltas, rivers, and lakes [29]. The Majiagou Formation mainly contains limestone and dolomite that were formed in a carbonate platform environment [30].

As a large sedimentary basin in the west of the North China block, the Ordos Basin has gone through five tectono-sedimentary stages, i.e., the Middle-Late Proterozoic aulacogen stage, the Early Paleozoic shallow marine platform stage, the Late Paleozoic littoral plain stage, the Mesozoic hinterland basin stage, and the Cenozoic peripheral faulted basin stage [31–33]. From the Middle-Late Proterozoic to Early Paleozoic, stable carbonate rocks of several kilometers' thick were deposited. During the early Ordovician, the uplift and depression patterns were formed in the Ordos Basin. The central paleo-uplift extended from Qingyang to the southeast (Figure 1). The depressions on both sides of the central paleo-uplift were characterized by an evaporative saline lake system with thick argillaceous dolomite, which was considered as the potential hydrocarbon source rock [34]. The slope belts on both sides of the central paleo-uplift were broad areas of tidal flat dolomite. Affected by the Caledonian tectonic movement, the Ordos Basin uplifted together with the North China block in the Middle-Late Ordovician, resulted in weathering and erosion at the top of Middle-Late Ordovician for 150 million years with well-developed dissolution pores and good reservoir performance. It is therefore the most favorable layer of a gas field and one of the main gas reservoirs found in the Ordos Basin. This tectonic movement caused the absence of the Late Ordovician-Early Carboniferous sediments in the Ordos Basin and even the whole North China block. It was not until the Middle-Late Carboniferous that the Ordos Basin and the North China block began to subside again. The seawater invaded from northeast to southwest, and the Ordos Basin and the vast areas of North China block as a whole exhibited a paleogeographic pattern of coexisted epeiric sea and delta, forming the coal-bearing deposits mixed with carbonate rocks and terrigenous clastics. In the regressive environment, the Permian sediments gradually evolved into lacustrine delta with thick deposition of dark organic-rich mudstone and coal-bearing sediments. These deposits are good natural gas source rocks and clastic reservoirs, which are the most important natural gas reservoirs that have been discovered by exploration so far [1].

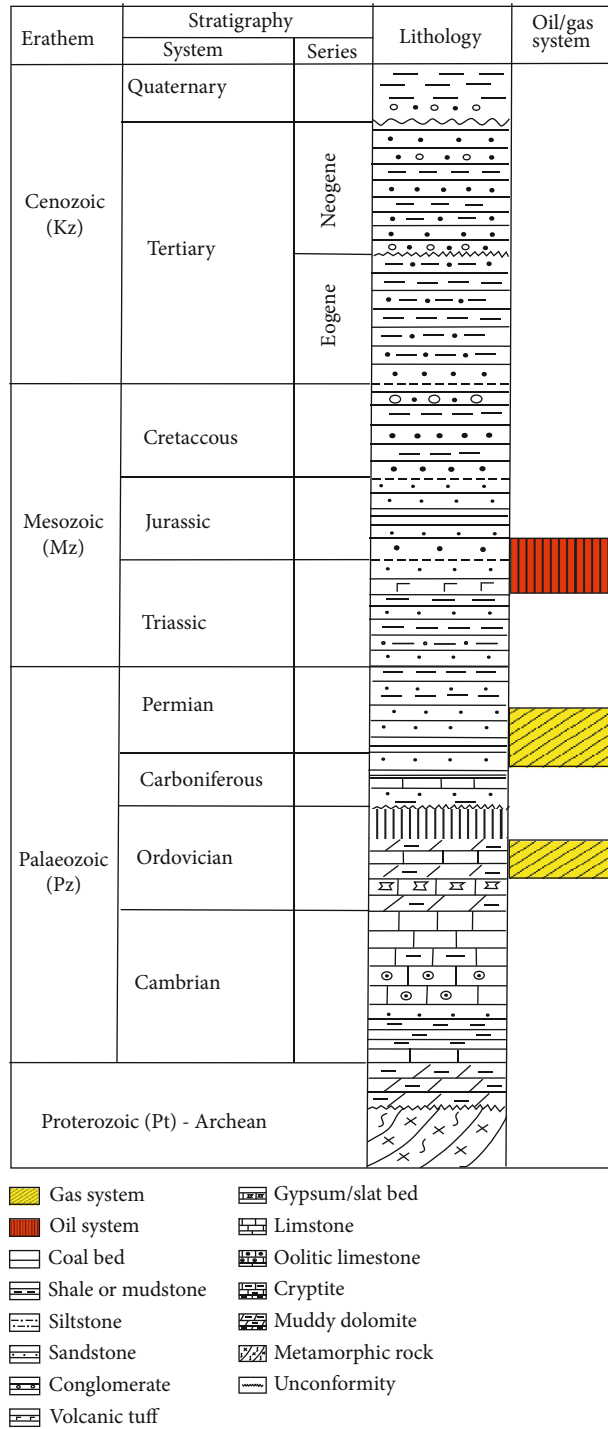
During Triassic, the Ordos Basin became a large-scale depression basin dominated by river-lake delta deposits, which constituted the major low-permeability oil and gas system in the Ordos Basin. At the end of the Late Triassic, due to the Indosinian movement, the collision between the North and South China blocks formed the Qinling Central Orogenic Belt, resulting in the uplift of the North China block. Hence, the Upper Triassic strata in the Ordos area experienced a long period of erosion, forming a wide range of valleys filled with Jurassic glutenite. The Yanshan movement at the end of the Jurassic led to the formation of large-scale nappes and thrust uplifts in the western and eastern margins of the basin. The main body of the basin formed an asymmetric east-west compressive syncline. The northern Ordos Basin remained as an uplift for a long time and was higher than the southern Ordos Basin. At the same time, the southern margin and eastern part of the basin uplifted as a whole. From the Cenozoic, the Paleozoic strata at the edge of the basin were exposed to the surface, while the fault



- | | | | | |
|--|---|--|----|---|
| | 1 | | 6 | 1. Cenozoic depression; 2 Ordos basin; 3. Upper paleozoic fluvial sand bodies; |
| | 2 | | 7 | 4. Upper paleozoic sandstone gas reservoir; 5. The dolomite gas reservoir of Ordovician Majiagou Formation; 6. Central palaeo-uplift; 7. Orogenic belt; |
| | 3 | | 8 | 8. Boundary line; 9. City; 10. Exploratory well |
| | 4 | | 9 | YB-Yinshan orogenic Belt DB-Daqingshen orogenic Belt HTG-He Tao Graben |
| | 5 | | 10 | HLS-HeLan Shan YCG-YinChuan Grabe QLB-QiLian orogenic Belt |
| | | | | QB-Qinling orogenic Belt WHG-WeiHe Graben FHG-FenHe Graben |
| | | | | NCB-North Chine Block |

(a)

FIGURE 1: Continued.



(b)

FIGURE 1: Structure and gas reservoir distribution of the Ordos Basin.

depressions around the basin formed a series of fault basins, in which the thickness of the Cenozoic strata exceeds 5000 m.

There are two sets of gas-bearing layers in the middle and southern part of the Ordos Basin, namely, the oil-type gas system of the Lower Paleozoic Ordovician marine carbonate rocks and the typical coal-derived gas system of the Permian mudstone and coal seam. The Upper Paleozoic

coal-bearing source rocks have diverse material sources and kerogen types. Generally, the coal seam has organic carbon content of 70.8%-83.2% and chloroform bitumen "A" content of 0.61%-0.80%, while the dark mudstone has organic carbon abundance of 2%-3% and chloroform bitumen "A" content 0.037%-0.120%. Most hydrocarbon source rocks were in the high/over mature stage with $R_o > 1.5\%$.

The Lower Paleozoic Ordovician hydrocarbon source rocks belong to type I and type II organic matter types, with moderate to good abundances and $R_o > 2.0\%$. The Ordovician system mainly consists of weathering crust type, dolomite type, and karst fracture-cavity type reservoirs, which can be divided into three major gas accumulation assemblages, the Ordovician weathering crust, the dolomite on the east of the paleo-uplift, and the karst fracture-cave type gas reservoir on the west of the paleo-uplift. The effective hydrocarbon source rocks in the Upper and Lower Paleozoic strata provided rich gas sources for the karst fracture-cavity traps and formed a good source-reservoir configuration.

3. Samples and Experiments

In this study, more than 50 sandstone core samples of the He 8 section and Shan 1 section were collected from several exploratory wells in the central paleo-uplift of the Ordos Basin (L1 well, Xt 1 well, Yt 1 well, U1 well, F1 well, F2 well, F3 well, Y2 well, S139 well, and S15 well). A total of 50 representative Paleozoic core samples around the central paleo-uplift of the basin were selected for analysis of fluid inclusions, including the core samples of the Permian sandstone reservoir and the Ordovician Majiagou Formation reservoir [35]. Firstly, the samples were made into 50 polished double-sided rock slices. A Leitz microscope was used to observe the petrographic characteristics of fluid inclusions, including color, size, occurrence, host minerals, and the gas-liquid ratio of fluid inclusions, with a lens combination of 10 times eyepiece and 50 times objective lens under the laboratory temperature of 26°C. The brine composition types of fluid inclusions were determined by measuring the initial melting temperatures of the inclusions. The fluid inclusions were placed on a heating and freezing stage until frozen and then slowly heated to record the initial melting temperature at the appearance of the first drop of the liquid phase. The initial melting temperature is related to the chemical properties of the saline system of the inclusion fluid and thus could reflect the properties of the ancient fluid. Different brine systems have different initial melting temperatures. The initial melting temperatures of the common NaCl-H₂O system, CaCl₂-H₂O system, and MgCl₂-H₂O system are -20.8°C, -49.8°C, and -33.6°C, respectively. Secondly, laser Raman spectrometry analyses on fluid inclusions were conducted using a Ramnor-u1000 laser Raman molecular microprobe manufactured by Jobin-Yvon Instruments, France. The experiment used an Ar+ laser with a wavelength of 514.5 nm and a power of 300 mW. The double monochromator slit was 450 μm, and the dispersion was 9.3 cm⁻¹/mm. The high voltage of the photomultiplier tube was 1530 V. The laboratory temperature was 22°C, and the humidity was 65%.

The compositions of natural gas in hydrocarbon-bearing inclusions of Permian sandstone and Ordovician carbonate rock samples were analyzed by a thermal explosion method. Firstly, the samples were crushed through 100-80 mesh sieves and cleaned repeatedly with alcohol and benzene-methanol mixed solution to remove surface-adsorbed hydrocarbons. After drying, the samples were put into a

quartz furnace and vacuumed and heated to 300°C causing the explosion of the inclusions and the release of the gas in the inclusions. The compositions and relative content of natural gas were analyzed by an HP 5890 GC gas chromatograph, and they were compared against the natural gas compositions obtained by gas logging. At the same time, CH₄ was separated, and $\delta^{13}C_1$ carbon and δD were, respectively, determined, which were compared with the isotopes of natural gas collected from the natural gas layer. The compositions and source characteristics of natural gas in the inclusions were therefore determined.

4. Results

4.1. Fluid Inclusions

4.1.1. Inclusion Types. Through microscopic petrographic observation, fluid inclusions in both the Permian sandstone and Ordovician Majiagou Formation dolomite reservoirs can be divided into two phases. The early-phase inclusions are gas-liquid two-phase inclusions containing liquid hydrocarbon and showing fluoresce, indicating that petroleum entered the reservoir in the early stage of the reservoir formation. The late-phase inclusions are gas-liquid two-phase inclusions containing gaseous hydrocarbons, recording gaseous hydrocarbon entering the reservoir in the late stage of reservoir formation. In the Permian sandstone reservoir, the early-phase gas-liquid two-phase inclusions containing liquid hydrocarbons are small and distributed along the early fractures of clastic particles and in the irregular dissolution pores at the edge of particles. In addition, many gas-liquid two-phase inclusions containing liquid hydrocarbon are in the dissolution pores of quartz particles. The liquid hydrocarbon phase emits weak yellow-green fluorescence under the fluorescence microscope (Figures 2(a), 2(b), 2(d), and 2(e)), but the gaseous phase does not emit fluorescence (Figures 2(c) and 2(f)). The late-phase gas-liquid two-phase inclusions containing gaseous hydrocarbons are distributed in a bead-like direction along the late-diagenetic fractures that cut through the particle boundary. The gaseous bubbles are grayish-black, and the gas/liquid ratios are generally about 20%. These inclusions do not emit fluorescence (Figures 2(c) and 2(f)).

The early-phase inclusions in the dolomite of the Middle Ordovician Majiagou Formation are gas-liquid two-phase inclusions containing liquid hydrocarbons and distributed in the dissolution pores of dolomite. The sizes of the inclusions are mostly 3-5 μm, and the gas/liquid ratios are 5%-10%. There is no fluorescence in the bubble center, whereas the liquid hydrocarbon phase distributed around the inclusions shows weak yellow-green fluorescence (Figures 3(a) and 3(b)). The late-phase inclusions are gas-liquid two-phase inclusions containing gaseous hydrocarbons and distributed in sparry calcite filled with dissolution pores. The bubbles of the inclusions are light gray, and the inclusions are large with sizes of 10-30 μm. These inclusions have varied gas/liquid ratios and do not emit fluorescence. Inclusions filled the cleavages of the calcite and showed angular shapes (Figures 3(c)-3(f)).

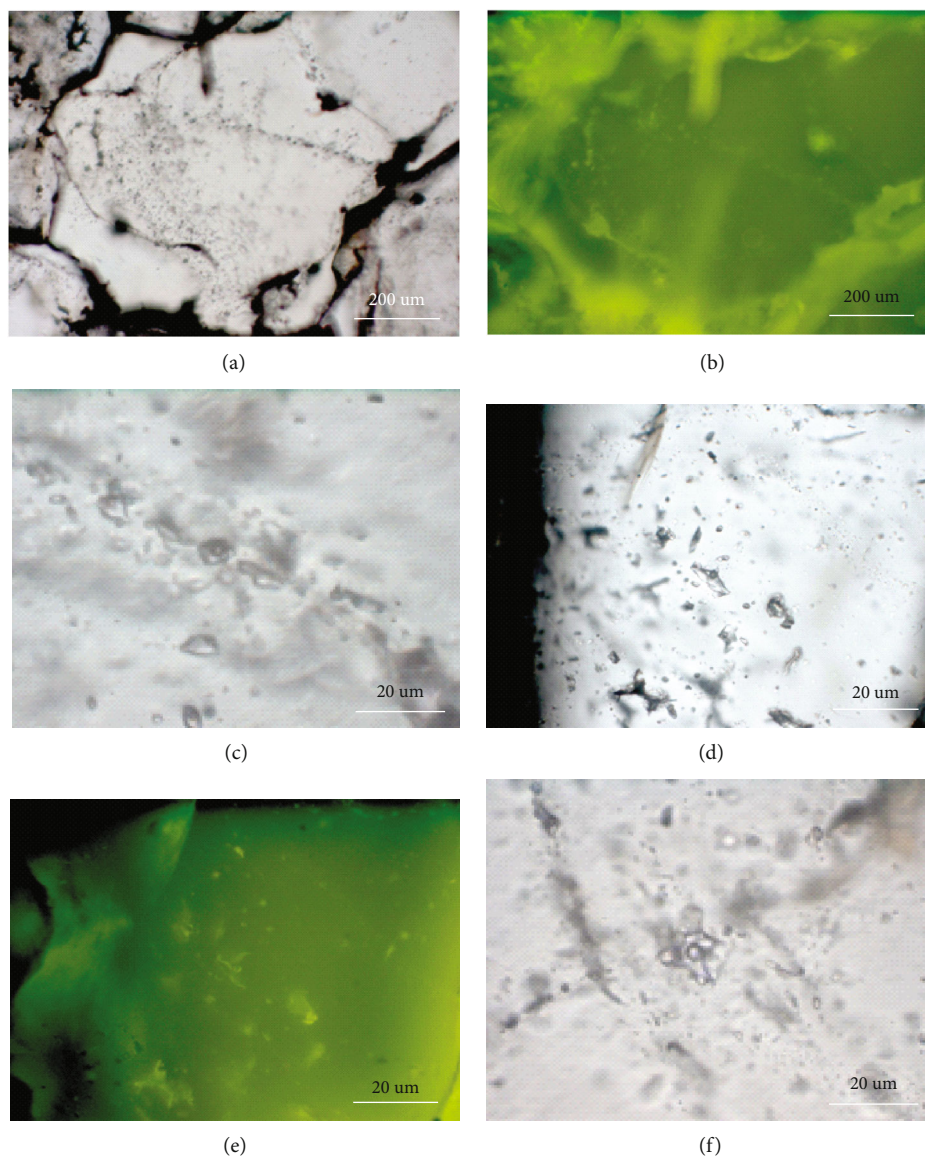


FIGURE 2: Microscopic photographs of Early and Late Paleozoic Permian sandstone inclusions. (a) Liquid hydrocarbon inclusions in early fractures and enlarged edges of quartz grains, F3 well, 2958.61 m, P_2 , (-); (b) the same field of view as (a), fluorescence; (c) gaseous hydrocarbon inclusions in late fractures of quartz grains, F2 well, 2753.87 m, P_2 , (-); (d) quartz particle dissolution pore fractures contain liquid hydrocarbon inclusions, F1 well, 2708.4 m, P_2 , (-); (e) the same field of view as (d), fluorescence; (f) gaseous hydrocarbon inclusions in late fractures of quartz particles, F2 well, 2753.87 m, P_2 , (-).

4.1.2. Inclusions Homogenization Temperature and Salinity.

Homogenization temperature and other parameters of fluid inclusions in the central-southern basin were measured by a heating and freezing stage. Both the Permian sandstone inclusions and Ordovician Majiagou Formation dolomite inclusions have two peak ranges of homogenization temperatures. The homogenization temperature peak ranges of the Permian sandstone inclusions vary from 110°C to 120°C and from 160°C to 170°C. The homogenization temperature peak ranges of the Ordovician dolomite inclusions are 120°C–130°C and 170°C–180°C (Figure 4), slightly higher than those of the Permian sandstone. Through microscopic observation, the low-temperature inclusions from either the Permian sandstone or the Ordovician carbonate rocks are

mostly early-phase liquid hydrocarbon inclusions with fluorescence, corresponding to the early formation of liquid hydrocarbon and migration into the reservoir. The high-temperature inclusions are mostly late-phase gaseous hydrocarbon inclusions without fluorescence, formed during the large-scale migration of natural gas into the reservoir.

The fluid salinity of fluid inclusions was then calculated. The salinity of fluid inclusions in the Permian sandstone varies from 0.2 wt% to 15.0 wt% but is generally low and concentrated in the range of 0.0–5.0 wt% (Figure 5). The salinity is generally low, and relatively few are higher than 5.0 wt%. The salinity of dolomite fluid inclusions in the Ordovician Majiagou Formation ranges from 1.0 wt% to 20.0 wt% with the peak interval from 1.0 wt% to 11.0 wt%,

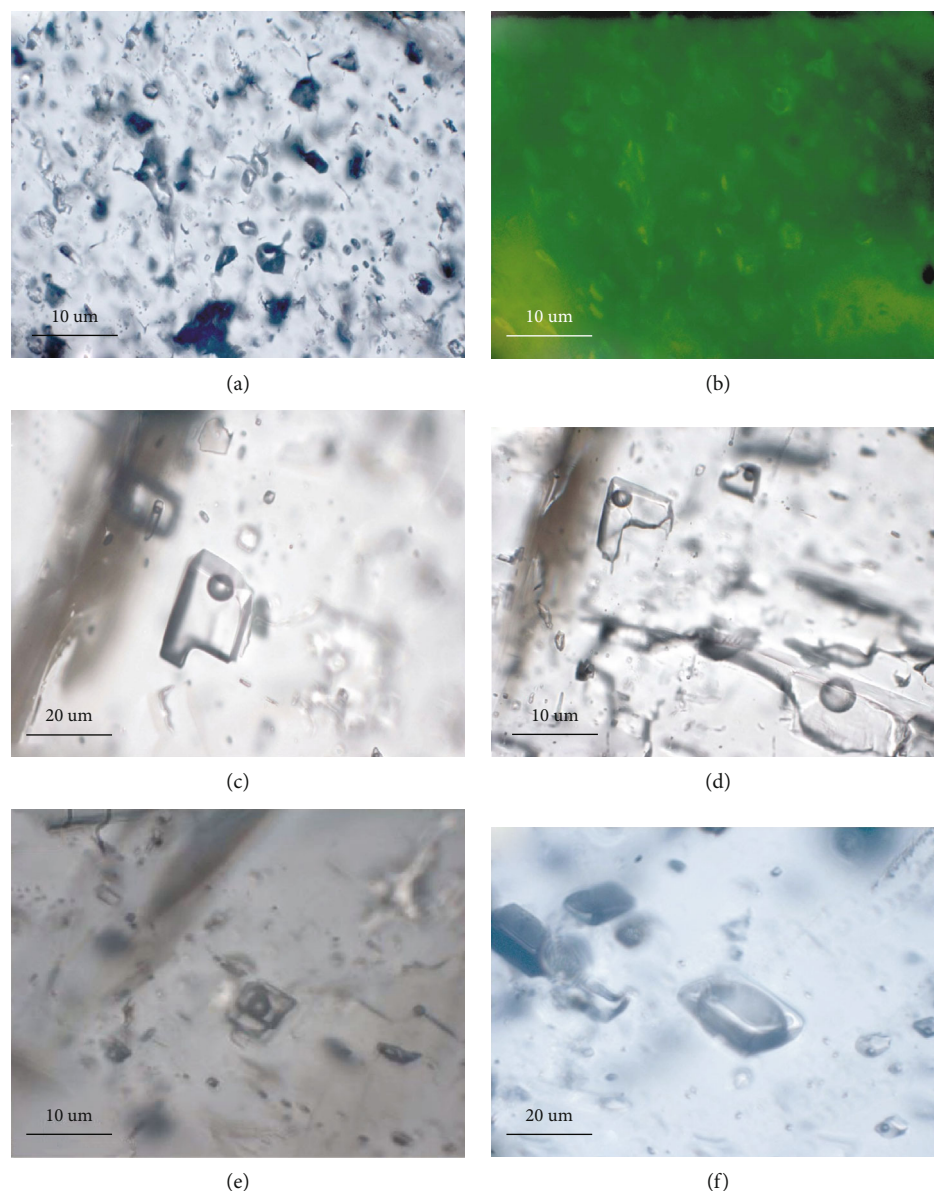


FIGURE 3: Microscopic photographs of early and late-stage inclusions in Ordovician Majiagou Formation dolomite. (a) Liquid hydrocarbon inclusions in dolomite dissolution pores, F6 well, 2770.9 m, O₂, (+); (b) the same field of view as (a), fluorescence microscope; (c, d) gaseous hydrocarbon inclusions in late bright crystal calcite filled with dissolution pores, Xt 1 well, 3297.5 m, O₂, (+); (e) gaseous hydrocarbon inclusions in late-stage calcite filled with dissolution pores, Y2 well, 2528.7 m, O₂; (f) methane-rich gas inclusions in bright crystal calcite, F6 well, 2770.9 m, O₂, (+).

which is generally higher than that of the Permian sandstone fluid inclusions. Combined with the petrographic observation, most fluid inclusions with high salinity are early-phase liquid hydrocarbon fluid inclusions, while most late-phase gaseous hydrocarbon fluid inclusions have relatively lower salinity.

4.1.3. Inclusions Composition. Through laser Raman microprobe analyses of fluid inclusions from the Permian and Ordovician Majiagou Formation, the contents of H₂O are generally between 50% and 70% in liquid inclusions and from 0% to 30% in gas inclusions, with CH₄, CO₂, H₂S, and other trace hydrocarbons. CH₄ content is the highest among all hydrocarbon gases, and its content in the gas

phase is obviously higher than that in the liquid phase. A comparison shows that the CH₄ contents and the CH₄/total hydrocarbon ($\sum\text{CH}$) ratios in the late-phase inclusions are significantly higher than those in the early-phase inclusions, indicating that the late-phase inclusions mainly recorded the organic matter composition during the main period of organic fluid migration. CH₄ contents in the gas phase of late-phase inclusions account for more than 92% of the total hydrocarbons, indicating that late-phase inclusions recorded fluid composition during the main accumulation period (Figure 6). The gas and liquid phases of the early and late inclusions of the Ordovician Majiagou Formation contain a certain amount of H₂S. The CH₄ contents in gas and liquid

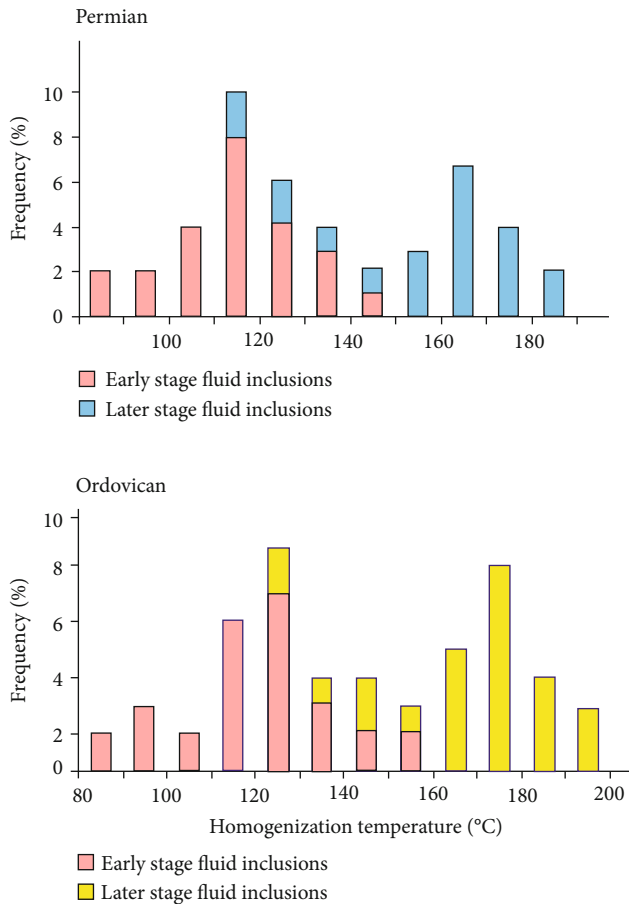


FIGURE 4: Uniform temperature distribution of inclusions.

phases show a positive correlation with the total hydrocarbon contents in the inclusions. With the increase of total hydrocarbon contents, the content of CH_4 also increases accordingly (Figure 7). It also proves that hydrocarbon-bearing inclusions are signs and records of hydrocarbon fluid migration.

The hydrocarbon components of the fluid inclusions were examined by thermal explosion of the fluid inclusions, and the results are shown in Table 1. The CH_4 contents in the hydrocarbon gases of the inclusions in the three carbonate samples of the Majiagou Formation are between 65.79% and 84.66%, while those in the two Permian sandstone samples are between 49.15% and 73.31%. In general, the characteristics of gaseous hydrocarbon compositions and contents in the inclusion samples analyzed by this method are generally consistent with those of individual inclusions analyzed by laser Raman (Figure 7), i.e., the methane content is the highest in all gaseous hydrocarbons.

4.1.4. Inclusions Isotopic Characteristics. The inclusions were opened to analyze the carbon and hydrogen isotopes of the wrapped methane, and the results are shown in Table 1. The methane gas $\delta^{13}\text{C}_1$ and $\delta\text{D}_{\text{SMOW}}$ of the inclusions in the Permian sandstone reservoir are significantly lower than those of the dolomite inclusions in the Majiagou Formation. The methane gas $\delta^{13}\text{C}_1$ of the inclusions in the Permian sandstone reservoir is between -30.22% and -29.63% ,

and the corresponding $\delta\text{D}_{\text{SMOW}}$ varies from -96.37% to -102.78% . The $\delta^{13}\text{C}_1$ of methane gas in dolomite inclusions of Majiagou Formation ranges from -33.29% to -37.76% , and the corresponding $\delta\text{D}_{\text{SMOW}}$ is between -128.3% and -132.19% .

4.1.5. Comparison of Gas Composition between Inclusions and Natural Gas in the Natural Gas Layer. The natural gas found in the Ordos Basin is mainly composed of methane (CH_4), and the content of heavy hydrocarbon (C_{2+}) is generally low, with a small amount of carbon dioxide, nitrogen and trace hydrogen [36, 37]. The Lower Paleozoic generally contains trace hydrogen sulfide gas. The methane (CH_4) content of natural gas in the Permian reservoir is between 85.619% and 98.62%, concentrating from 92% to 96% with an average of 93.82%. The methane content in the Ordovician Majiagou Formation is between 87.38% and 98.37%, mainly from 92% to 97% with an average of 94.39% [36, 37].

Since natural gas inclusions were captured during the large-scale migration and accumulation of natural gas, the gaseous hydrocarbon components in these inclusions should be similar to those in the natural gas reservoirs. This study analyzed and compared the gas composition of the gas layer of the Ordovician Majiagou Formation in the F6 well, the gas composition obtained by gas logging in this gas-bearing interval (2770.07–2770.89 m), and the gas composition of inclusions in this layer obtained by thermal explosion method (Table 2). The results show that the main hydrocarbon gas composition of the three is CH_4 , and the content of heavy hydrocarbon gas is very low (Figure 8). The natural gas layer has the highest (>94%) CH_4 content. The CH_4 contents of natural gas measured by gas logging and of the same-layer inclusions are relatively low (less than 80%), and heavy hydrocarbon gas is more than 20%. These indicate that the compositions of natural gas in the inclusions are different from those in the natural gas layer. The reason is the natural gas compositions captured in the inclusions represent the compositions of the original natural gas during the large-scale migration and accumulation period, in which the gas-moisture differentiation was incomplete and the inclusion compositions remained unchanged after being captured. Comparatively, natural gas in the gas layer experienced complex changes in the later period, including secondary differentiation of gas and water after accumulation.

5. Discussion

5.1. Analysis of Natural Gas Source Rock. The hydrocarbon source rocks and genesis of the natural gas in the Ordos Basin are controversial. It is generally believed that the coal-bearing rocks in the Upper Paleozoic are the main hydrocarbon source rocks [29, 36]. Natural gas exploration has been carried out around coal-bearing rocks for a long time, and several large natural gas fields have been found around the hydrocarbon generation center of the Upper Paleozoic coal-bearing rocks in the northern basin. In recent years, many scholars have noticed the contribution of Ordovician marine rocks to hydrocarbon generation. Through the study on the distribution of Ordovician marine rocks,

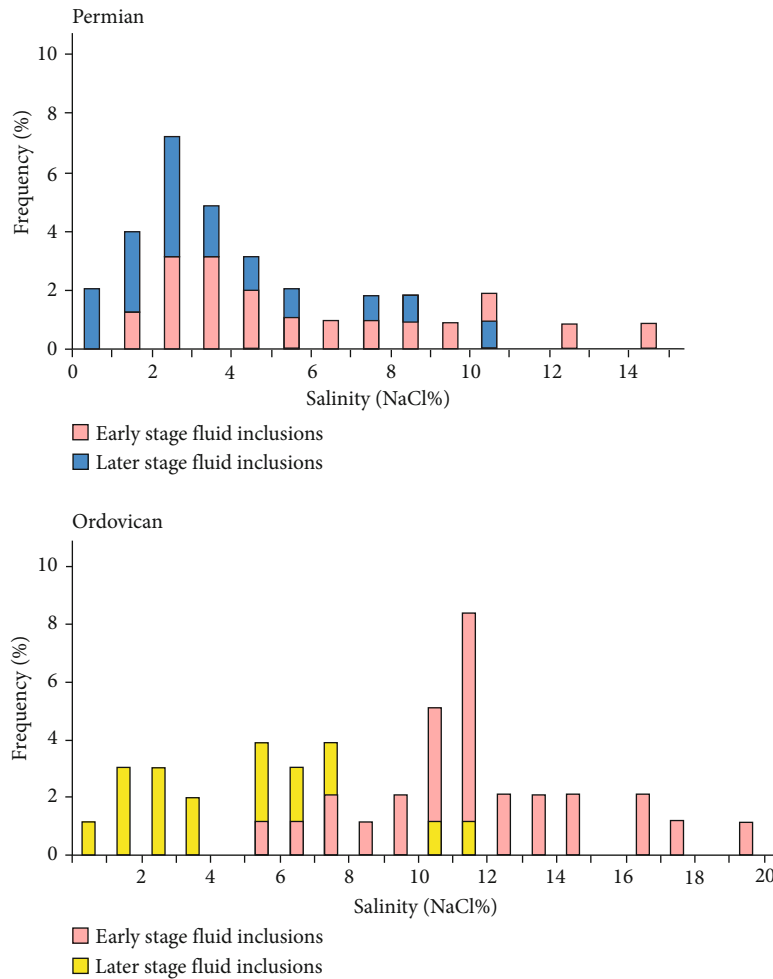


FIGURE 5: Salinity components of fluid inclusion.

organic geochemistry of rocks, natural gas composition, and isotope geochemistry, it is considered that the dark stratiform mudstone, dolomitic mudstone, and argillaceous dolomite of the Ordovician Majiagou Formation are also effective hydrocarbon source rocks [38].

The carbon and hydrogen isotopes of methane in natural gas inclusions in different layers are different. Methane isotopes of natural gas inclusions in different layers in Table 1 show the methane $\delta^{13}\text{C}_1$ in the inclusions of the Permian sandstones varies from -30.22‰ to -29.63‰ , and the methane $\delta^{13}\text{C}_1$ in the inclusions of the Ordovician Majiagou Formation dolomite ranges from -33.29‰ to -37.76‰ . Compared with the methane $\delta^{13}\text{C}_1$ in the natural gas, the gas layer of weathering crust, and the gas layer beneath the weathering crust of the Ordos Basin (Table 3) summarized by Dai et al. [39], the methane $\delta^{13}\text{C}_1$ in the inclusions of the Permian Shanxi Formation sandstone is consistent with that in the Carboniferous-Permian gas layer of the Ordos Basin, while the methane $\delta^{13}\text{C}_1$ in the Ordovician Majiagou Formation is consistent with that in the gas layer of weathering crust in Ordos Basin.

The natural gas $\delta^{13}\text{C}_1$ of the inclusion from Majiagou Formation dolomite in F6 well is much closer to that of the Majiagou Formation compared to that of other different

gas layers in the well area (Table 4), indicating that the inclusions recorded the characteristics of the natural gas accumulation.

On the genetic discrimination diagram of natural gas $\delta^{13}\text{C}_1$ - δD of Schoell [40] (Figure 9), the natural gas inclusions from different wells and different layers plot in different genetic fields but all in the dry gas field, corresponding to a thermal evolution degree with R_o greater than 2.0%, which is consistent with that of the natural gas hydrocarbon source rocks in this region. Inclusions in the Permian sandstone of the Shanxi Formation are located in the dry gas area of humic pyrolysis, indicating the natural gas wrapped in the sandstone was derived from the Carboniferous-Permian coal-bearing strata. Inclusions in the Ordovician dolomite fall in the mixed dry gas area, suggesting the natural gas was derived from the Upper Paleozoic coal-bearing strata and the Lower Paleozoic carbonate rocks. Therefore, the inclusion isotopes show natural gas originated from both Permian coal-bearing rocks and Ordovician carbonate rocks.

5.2. Fluid Characteristics. Fluid inclusions are widely distributed in petroliferous basins. The fluid system in inclusions is used to trace the ancient fluid migration as it is the only observable primary fluid sample for hydrocarbon migration

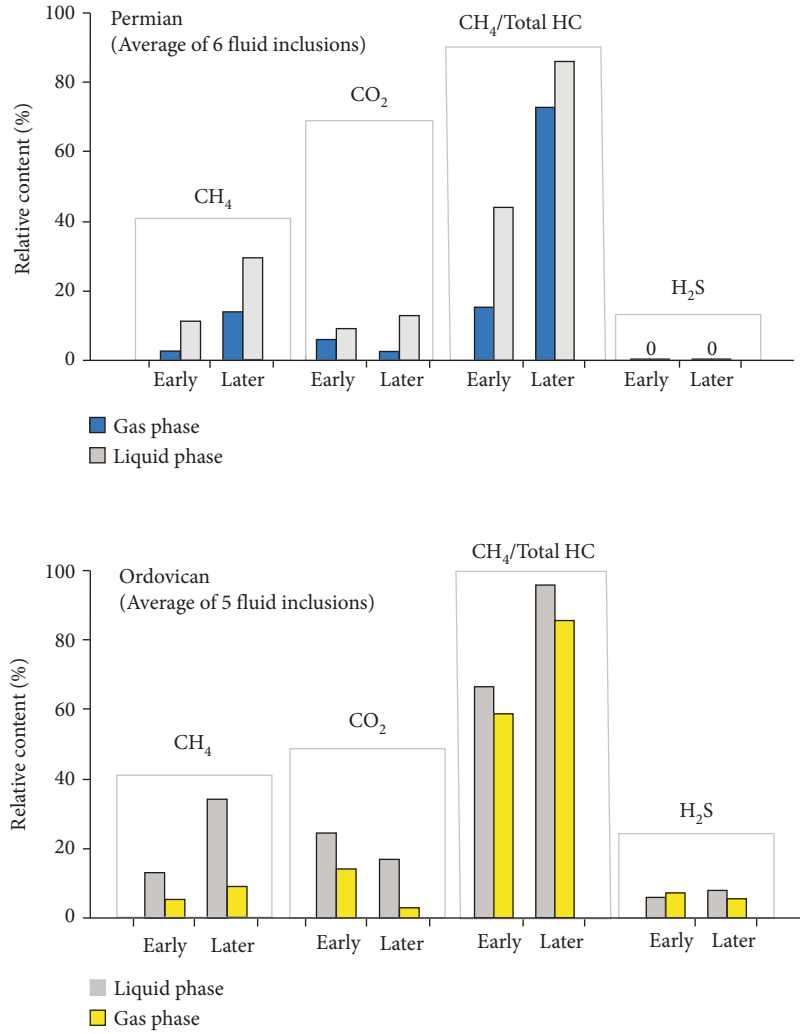


FIGURE 6: Comparison of mean values of main components in gas and liquid phases of inclusions by laser Raman spectroscopy.

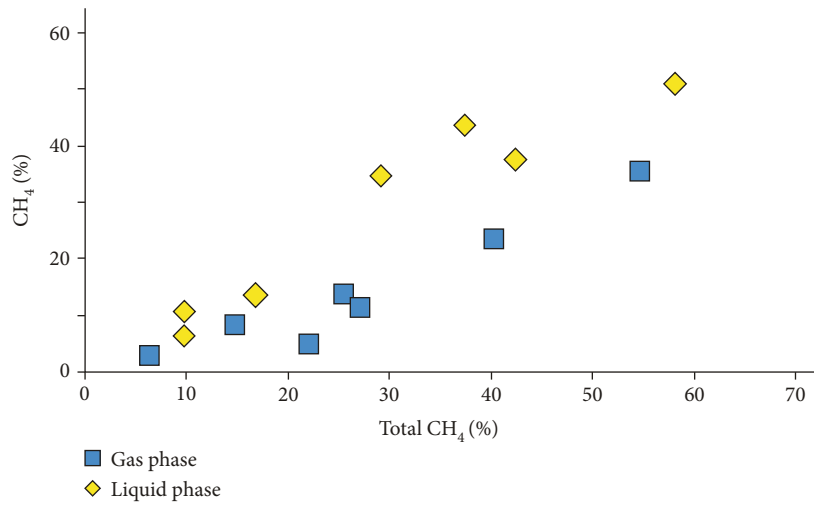


FIGURE 7: Relationship between the content of gas, liquid methane in inclusions, and total hydrocarbon in laser Raman analysis.

TABLE 1: Results of gaseous hydrocarbon composition and methane isotope analysis of inclusions analyzed by inclusion opening method.

Sample	Lithology	Stratum/depth	Composition	C ₁	C ₂	C ₃	C ₄	C ₅	∑C _i	δ ¹³ C ₁	δD _{SMOW}
L1 well	Sandstone	Shanxi Formation/3424.08	a	0.8132	0.4051	0.2071	0.143	0.086	1.6544	-29.63	-102.78
			b	49.15	24.49	12.52	8.64	5.20	100		
	Dolomite	Majiagou Formation/3563.50	a	1.9616	0.6461	0.1664	0.1172	0.0905	2.9818	-33.29	-128.3
			b	65.79	21.67	5.58	3.93	3.04	100		
Xt 1 well	Dolomite	Majiagou/	a	1.8946	0.1947	0.1007	0.0568	0.0118	2.2586	-37.76	-132.19
			b	83.88	8.62	4.46	2.51	0.52	100		
Y2 well	Sandstone	Benxi Formation/2503.1	a	2.0206	0.4514	0.1621	0.1074	0.0146	2.7561	-30.22	-96.37
			b	73.31	16.38	5.88	3.90	0.53	100		
F6 well	Dolomite	Majiagou Formation/2770.9	a	1.8991	0.2191	0.1434	0.0861	0.041	2.3887	-33.35	-111.03
			b	79.51	9.17	6.01	3.60	1.72	100		
			2770.17-2770.89	c	77.49	21.77	0.37	0.37	0.00	100	—

Note: a: gas content, unit: m³/t rock; b: relative content, Ci/Ci (×100%); c: relative gas content, %, obtained from gas logging in well section 2770.17-2770.89 m.

TABLE 2: Comparison of hydrocarbon composition (%) of natural gas inclusions and gas logging in Majiagou Formation of F6 well.

Gas layer	Depth (m)	Composition (%)	C ₁	C ₂	C ₃	C ₄	C ₅	∑C _i
	2770.07-2770.89		94.26	3.57	1.74	0.43	0	100
Dolomite inclusions	2770.9	Gas content (m ³ /rock)	1.8991	0.2191	0.1434	0.0861	0.041	2.3887
		Relative content (%)	79.51	9.17	6.01	3.60	1.72	100
Gas logging	2770.07-2770.89	Content (%)	1.121	0.126	0.055	0.002	0.002	1.326
		Relative content (%)	77.49	21.77	0.37	0.37	0.00	100

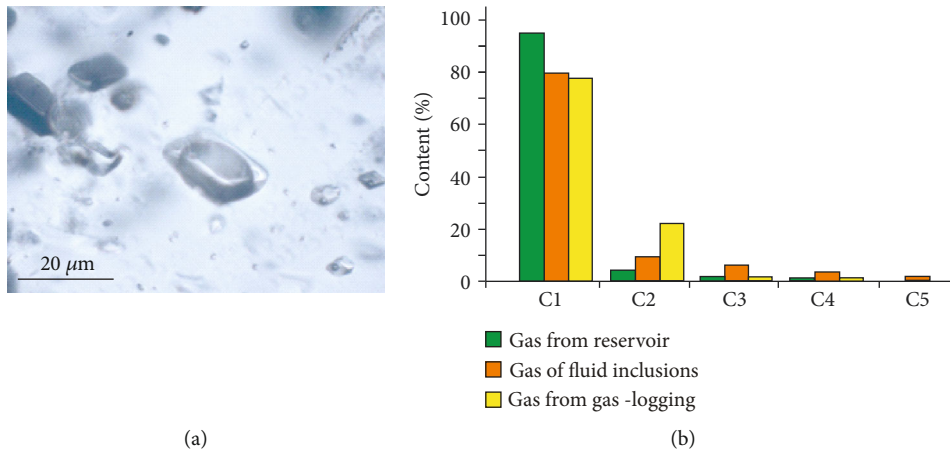


FIGURE 8: Comparison of gas compositions among Majiagou Formation gas layer, gas logging, and the same-layer fluid inclusions.

and accumulation. The common fluid inclusion brine systems are NaHCO₃ type water, CaCl₂ type water, Na₂SO₄ type water, MgCl₂ type water, and NaCl type water. NaHCO₃ type water is a common type of semiclosed oilfield water, and it is a direct sign of oil when the total salinity of the water is high and Cl⁻ and HCO₃³⁻ are dominant in water. CaCl₂ type water is also common in oilfield water. Generally, in a reservoir with a stable geological structure of good sealing and interlayer separation, CaCl₂ type water is dominant and directly signifies oil. Na₂SO₄ type water is rare in oilfield water, and the oil-bearing prospect is not ideal. In the gas field, Na₂SO₄ type water is hardly seen and NaHCO₃ type

water is predominant. MgCl₂ type water has marine geochemical characteristics and is not an oil-bearing marker under normal conditions. NaCl type water is widely distributed in oilfield.

Fluid inclusion analysis shows that the peak homogenization temperatures of the Permian sandstone inclusions are 110°C-120°C and 160°C-170°C, while those of the Ordovician dolomite inclusions are 120°C-130°C and 170°C-180°C. The peak salinity of fluid inclusions in the Permian sandstone is from 0.0 wt% to 5.0 wt %, and that of the fluid inclusions in the Ordovician Majiagou Formation dolomite is between 1.0 wt% and 11.0 wt%. The diagenetic fluid is in

TABLE 3: Statistical values of natural gas methane isotopes in different layers of the Ordos Basin [39].

Stratum	$\delta^{13}C_1$ (‰)	
	Range	Average value (amount)
Carboniferous-Permian gas layer	-37.3~-25.5	-33.4 (44)
Gas layer of weathering crust	-36.9~-29.0	-33.6 (90)
The gas layer beneath the weathering crust	-40.8~-37.2	-38.9 (7)

TABLE 4: Comparison of carbon isotopes of inclusions in Fugu 6 well in different gas layers in the well area.

Sample	Stratum/depth (m)	$\delta^{13}C_1$ (‰)
Dolomite inclusions	Majiagou Formation/2770.9	-33.35
Gas	Shanxi Formation	-31.8
Gas	Majiagou Formation	-34.4

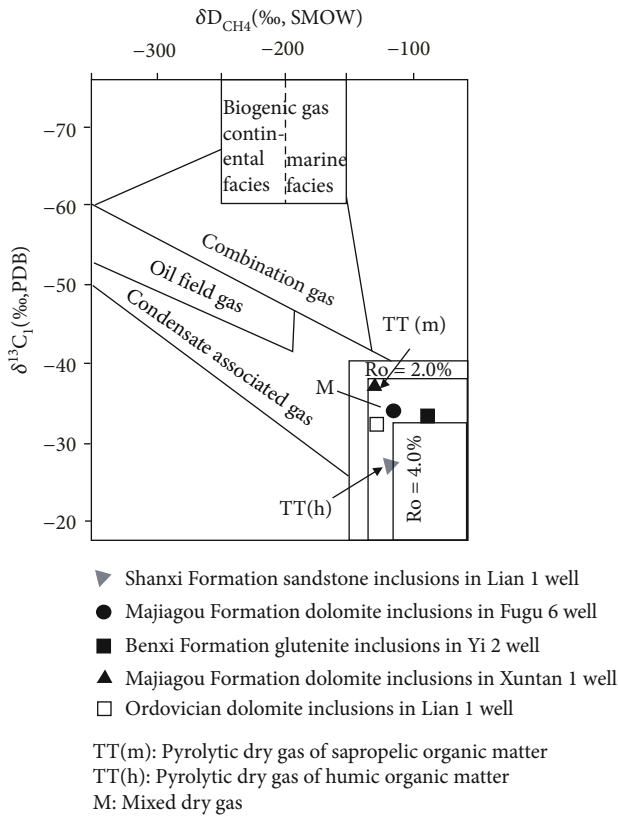


FIGURE 9: Genetic map of natural gas inclusions in the study area.

the range of medium-low temperature and moderate-low salinity [41]. According to the varying characteristics of fluid inclusion brine systems in the Permian and Ordovician strata of different wells in the study area (Figures 10 and 11), the fluid inclusion brine system in the Permian sandstones is mainly $MgCl_2$ - $NaCl$ - H_2O and subordinate $CaCl_2$ - H_2O . The brine system of fluid inclusions in the Ordovician dolomite is mainly $CaCl_2$ - $NaCl$ - H_2O , followed by the $CaCl_2$ - H_2O brine system, and rare $MgCl_2$ - H_2O system. In short, the brine system of fluid inclusions in the Ordovician is mainly a $CaCl_2$

brine system, indicating the hydrogeological stagnant conditions of the Ordovician were conducive to the existence of oil and gas. The brine of fluid inclusions in the Permian is mainly $MgCl_2$ - $NaCl$ - H_2O , which was not conducive to the existence of oil and gas. The formation and migration conditions of natural gas in the Lower Paleozoic were better than those in the Upper Paleozoic.

5.3. Accumulation Characteristics. The process of hydrocarbon accumulation is the formation and continuous injection of oil and gas fluid into the reservoir, displacing the primary pore water in the reservoir and finally accumulating [35]. Before oil and gas were injected into the reservoir, the reservoir pores were mainly occupied by the primary formation water. With the formation and entry of oil and gas into the reservoir, the primary fluid in the reservoir pores was displaced and replaced by oil and gas fluid. The fluid inclusions formed during this process contained oil and gas. Meanwhile, there was a coexistence of brine inclusions and liquid hydrocarbon inclusions [35, 42, 43]. Previous studies have shown the Upper Paleozoic coal-bearing hydrocarbon source rocks in the Ordos Basin produced mainly natural gas but no liquid hydrocarbons [44, 45]. This study has found that the early-phase inclusions in the Permian and Ordovician reservoirs contain liquid hydrocarbons with weak fluorescence, confirming the natural gas in the Ordos Basin experienced a liquid hydrocarbon formation stage [18]. It is consistent with the thermal evolution process of kerogen hydrocarbon generation of hydrocarbon source rocks. Liu et al. [29] and other studies have also found liquid hydrocarbon inclusions in the Paleozoic of the Ordos Basin and proposed that the formation of natural gas in the Ordos Basin experienced a process from liquid hydrocarbon to gaseous hydrocarbon. They believed the central-southern regions of the basin entered the oil generation stage in the Middle-Late Triassic, and the crude oil filled the central region in the early Middle Jurassic, forming liquid hydrocarbon inclusions with blue fluorescence and minor yellow fluorescence. However, at this time, industrial reservoirs were not formed. A large number of natural gas was generated in the middle of the Early Cretaceous and filled from south to the northern part of the Yishan slope and continued to form large-scale reservoirs before the uplift in the late Early Cretaceous. In this study, the inclusion lithofacies and compositional analysis have further proved that the natural gas reservoirs in Ordos Basin experienced an early liquid hydrocarbon formation stage, and the large-scale migration of natural gas was related to the development of late tectonic fractures.

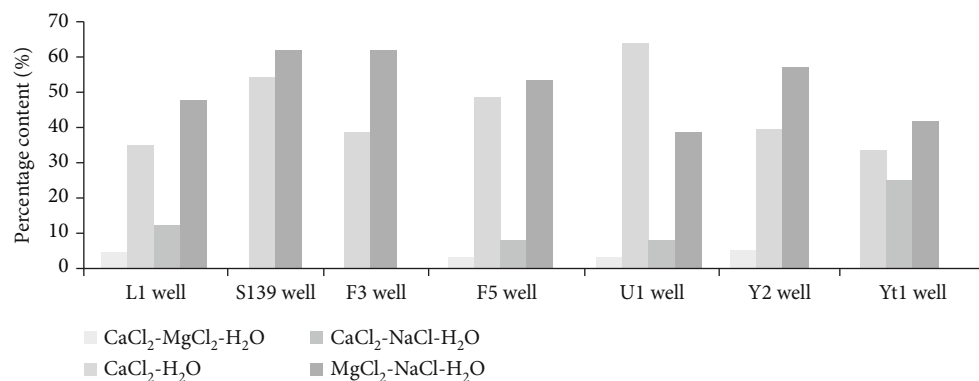


FIGURE 10: Characteristics of brine system of Upper Paleozoic inclusions.

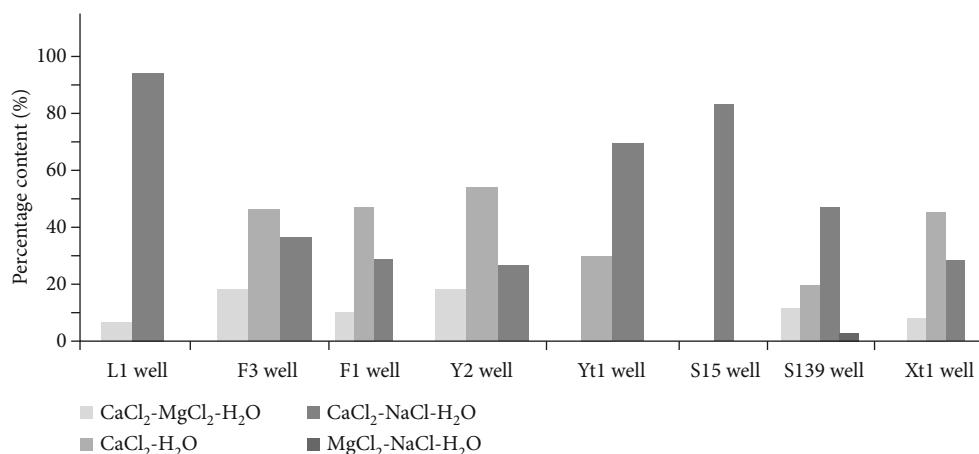


FIGURE 11: Characteristics of brine system of Lower Paleozoic inclusions.

TABLE 5: Rb/Sr isotope ratio analysis of the Permian fluid inclusions in F1 well.

Position	Depth (m)	Sample	Rb ($\mu\text{g/g}$)	Sr ($\mu\text{g/g}$)	$^{87}\text{Rb}/^{86}\text{Sr}$	$^{87}\text{Sr}/^{86}\text{Sr}$	Precision
Upper Shihezi Formation	2708.40	F2-1	0.008	0.122	0.1896	0.7154	± 0.000027
Upper Shihezi Formation	2711.20	F2-2	0.005	0.081	0.17834	0.71275	± 0.000034
Upper Shihezi Formation	2712.13	F2-3	0.005	0.075	0.18457	0.71454	± 0.000015
Shanxi Formation	3016.86	F2-4	0.006	0.168	0.17371	0.71266	± 0.000023
Shanxi Formation	3017.11	F2-5	0.006	0.08	0.19474	0.71593	± 0.000043

The Rb/Sr isotope method was used to date the age of fluid inclusions. The hydrocarbonaceous inclusions in the Permian sandstone of the F1 well are well-developed and dominated by the late gaseous hydrocarbon inclusions filled in fractures. The Rb-Sr isochron age of fluid inclusions represents the isotopic homogenization age of fluid and surrounding rock when the inclusions were formed, that is, the formation age of inclusions. To determine the age of fluid inclusions by Rb/Sr dating, the prerequisite is synchronous inclusions with the initial Sr isotopes reaching complete homogenization. In other words, the fluid in a group of fluid inclusion samples is homologous and synchronous. After the formation of fluid inclusions, the Rb/Sr isotope system should remain closed. The Rb/Sr ratios in a group of fluid inclusions that meet the prerequisite should be consistent and will plot on the same line in the Rb/Sr coor-

dinates. The slope of the line represents the change of the Rb/Sr ratio, which can determine the reliable formation age of fluid inclusion. The Rb/Sr isochron age of fluid inclusions was analyzed by selecting the mineral fluid inclusions developed in late-phase gas inclusions at different depths of the Permian strata in the F1 well. The results show the Rb/Sr isotope ratios of the five samples are relatively uniform (Table 5) with a good linear relationship (Figure 12), indicating the Sr isotopes of fluid inclusions in the selected samples reached homogenization and the Rb/Sr isotope system maintained a good sealing after the formation of fluid inclusions. The age of the determined fluid inclusions is 89.18 Ma, which represents the timing of the inclusions capturing the gas-bearing hydrocarbon fluids, namely, the age of natural gas accumulation.

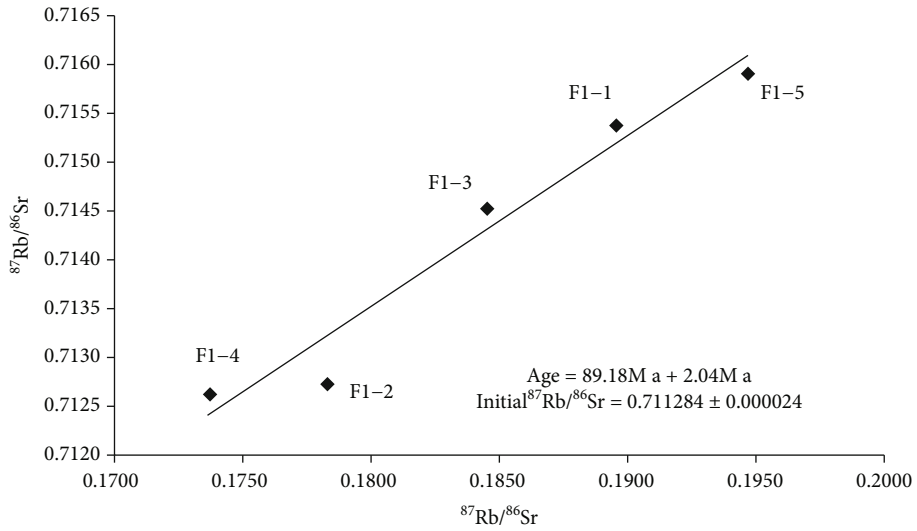


FIGURE 12: Rb/Sr isochron ages of fluid inclusions.

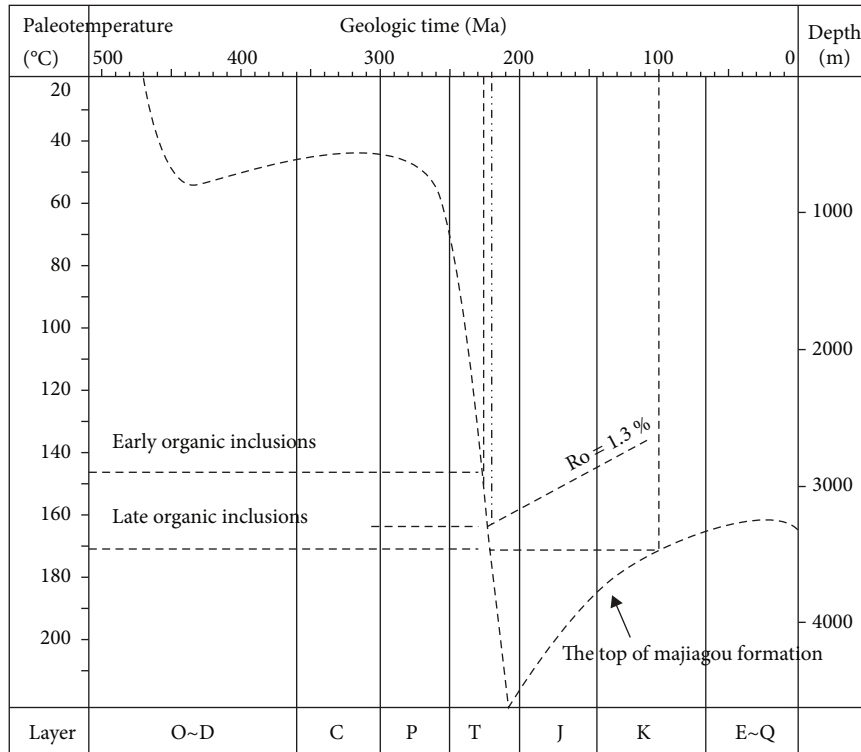


FIGURE 13: Gas accumulation time of Majiagou Formation of Xt 1 well in the Ordos Basin.

According to the homogenization temperatures of fluid inclusions, combined with the paleogeothermal and sedimentary tectonic evolution history of the basin, the formation time of inclusions can be determined, and then the formation time of natural gas reservoirs can be determined. This method is also called the “fluid inclusion method” for determining oil and gas accumulation [46–49]. According to the tectonic evolution history of the Ordos Basin, the representative Xt 1 well with complete stratigraphic data was selected to establish the burial depth-thermal evolution

curve of the Permian and Ordovician in the study area (Figure 13). The homogenization temperature method of inclusions was used to determine the time of natural gas migration and accumulation. Stratigraphic stratification of the Xt 1 well was based on the stratification data from the Changqing Oilfield Research Institute, and the strata erosion thickness and paleogeothermal gradient are based on references [50].

The inclusions in the temperature range of 145°C–155°C are the early-phase gas-liquid two-phase inclusions containing

liquid hydrocarbons, indicating the thermal evolution of the hydrocarbon source rocks was in the stage of liquid hydrocarbon generation. At this time, the thermal evolution was below the gas generation window ($R_o = 1.3\%$) (Figure 13). The inclusions in this stage recorded the early filling of liquid hydrocarbon-containing organic fluid into the reservoir. The homogenization temperature of the inclusions in this period intersects the burial section of the burial depth-thermal evolution curve of the Permian strata at the Late Triassic (220 Ma), when the fluid containing liquid hydrocarbon formed and began to enter the reservoir. The inclusions in the high-temperature range of 160°C – 170°C are gaseous hydrocarbon inclusions. At this time, the thermal evolution of hydrocarbon source rocks entered the gas generation window (Figure 13). The inclusions in this period were formed during the large-scale migration and accumulation of natural gas and were distributed in the late structural fractures. The homogenization temperature of these inclusions intersects the uplift section of the burial depth-thermal evolution curve of the Ordovician strata at the early Late Cretaceous (100 Ma), which is the time of natural gas accumulation in the Ordovician.

Combined with the burial thermal evolution history of the Xt 1 well (Figure 13), the gas accumulation process of the Majiagou Formation in the Ordos Basin was analyzed. Sedimentation occurred in the Middle and Late Ordovician, and then the carbonate rocks of the Lower Ordovician Majiagou Formation experienced a long period of weathering and erosion for about 150 Ma. Hence, the weathering crust reservoirs were formed [14]. Subsidence started in the Permian and lasted till the Late Triassic, with the burial depth increase of about 3900 m and the paleogeotemperature up to 145°C – 150°C . During this period (220 Ma), the hydrocarbon source rocks of Majiagou Formation entered the oil generation window and began to discharge hydrocarbons. The generated oil migrated along the weathering surface. The R_o reached the lower limit of the gas generation window of 1.3%, and thus, the oil began to transform into natural gas. At about 210 Ma, the paleogeotemperature of the strata reached 220°C , and a large quantity of oil and gas were accumulated. Due to the Yanshan movement, the strata were uplifted and resulted in a large number of structural fractures, which served as channels for oil and gas migration and accumulation space. After that, the strata were eroded due to the Himalayan movement. Till the Cenozoic, the burial depth of the strata was about 3300 meters. During this period, the formed oil and gas escaped along fractures, and the hydrocarbon generation gradually weakened to the end. The karst paleogeomorphology reservoirs of the Lower Ordovician Majiagou Formation in central Ordos Basin provided a good space for natural gas accumulation.

6. Conclusion

- (1) There are early- and late-phase organic fluid inclusions in the Upper Paleozoic Permian sandstone and the Lower Paleozoic Ordovician Majiagou Formation dolomite reservoirs. The early-phase

inclusions are gas-liquid two-phase inclusions containing liquid hydrocarbons with fluorescence, recording the petroleum entering the reservoir in the early stage of the reservoir formation. Late-phase inclusions are gas-liquid two-phase inclusions containing gaseous hydrocarbons, recording gaseous hydrocarbon migrating into the reservoir in the late stage of accumulation. Methane is the most abundant gaseous hydrocarbon in the inclusion

- (2) The Upper Paleozoic sandstone inclusions have peak homogenization temperature ranges of 110 – 120°C and 160 – 170°C , and the salinity peak range is 0.0 – 5.0 wt%, while the lower Paleozoic dolomite inclusions have peak homogenization temperature ranges of 120 – 130°C and 170 – 180°C and the peak salinity range of 1.0 – 11.0 wt%. The diagenetic fluid was in the range of medium-low temperature and medium-low salinity. The brine system of Ordovician fluid inclusions was dominated by CaCl_2 – H_2O , and the brine system of Permian fluid inclusions was mainly MgCl_2 – NaCl – H_2O . The conditions for the formation and migration of natural gas in the Ordovician were better than those in the Permian
- (3) Methane is the most abundant gaseous hydrocarbon in the inclusion. The formation of natural gas experienced a process from liquid hydrocarbon to gaseous hydrocarbon. The large-scale migration of natural gas was related to the development of late tectonic fractures. Both the coal-bearing rocks of the Permian and the carbonate rocks of the Ordovician were hydrocarbon source rocks for natural gas in the Ordos Basin
- (4) The time of accumulation was determined by Rb/Sr isotopic dating and the inclusion homogenization temperature method. The analysis of the gas formation process indicates that the process of the early-phase liquid hydrocarbon formation and migration into the reservoir corresponded to 220 Ma (Late Triassic). The late large-scale migration and accumulation of natural gas occurred at 100 Ma (early Late Cretaceous), which was close to the inclusion Rb/Sr isochron age of 89.18 Ma, indicating that the natural gas accumulation was related to the Yanshanian tectonic movement

Data Availability

Fluid inclusion homogenization temperature, salinity data, laser Raman spectroscopy analysis data, and gas chromatograph analyses used to support the findings of this study are included within the article.

Conflicts of Interest

The authors declare that they have no conflicts of interest.

Acknowledgments

This study was supported by the National Natural Science Foundation of China (number: 41772118) and the Fundamental Research Funds for the Central Universities, Chang'an University (No. 300102279106).

References

- [1] H. Yang, X. S. Liu, and X. X. Yan, "Tectonic-sedimentary evolution and tight sandstone gas accumulation in Ordos Basin since Late Paleozoic," *Earth Science Frontiers*, vol. 22, no. 3, pp. 174–183, 2015.
- [2] H. Yang, J. H. Fu, and X. S. Wei, "Characteristics of natural gas accumulation in Ordos Basin," *Natural Gas Industry*, vol. 25, no. 4, pp. 5–8, 2005.
- [3] H. Yang, J. H. Fu, X. S. Liu, and P. L. Mei, "Accumulation conditions and exploration and development of Upper Paleozoic tight gas in Ordos Basin," *Petroleum Exploration and Development*, vol. 39, no. 3, pp. 295–303, 2012.
- [4] H. Yang, X. S. Liu, and D. F. Zhang, "Main controlling factors and exploration progress of natural gas accumulation in Ordovician marine carbonate rocks in Ordos Basin," *Natural Gas Industry*, vol. 33, no. 5, pp. 1–12, 2013.
- [5] J. H. Fu, H. F. Bai, L. Y. Sun, and Z. R. Ma, "Types and characteristics of Ordovician carbonate reservoirs in Ordos Basin," *Acta Petrolei Sinica*, vol. 33, no. 2, pp. 110–117, 2012.
- [6] X. S. Liu, Y. L. Jiang, Y. D. Hou et al., "Genesis of combinatorial natural gas and its main controlling factors in Ordovician in Jingxi area of Ordos Basin," *Natural Gas Industry*, vol. 36, no. 4, pp. 16–26, 2016.
- [7] X. Li, *Study on the Characteristics and Thermal Evolution History of Paleozoic Source Rocks in Southeastern Ordos Basin*, [M.S. thesis], Chang'an University, 2007.
- [8] D. Liu, W. Z. Zhang, Q. F. Kong, Z. Q. Fen, C. C. Fang, and W. L. Peng, "The source rocks of Lower Paleozoic and natural gas causes in the Ordos Basin," *Petroleum Exploration and Development*, vol. 43, no. 4, pp. 540–549, 2016.
- [9] Z. J. Wang and X. S. Xu, "Discussion on gas source of Lower Paleozoic reservoir gas in Ordos Basin," *Sedimentary Geology and Tethyan Geology*, vol. 23, no. 4, pp. 84–90, 2003.
- [10] H. X. Cao, H. Y. Wu, X. M. Ren, Y. Wu, Q. S. Liang, and M. B. Tong, "The Ordovician karst paleomorphology and reservoir distribution in the southeast of Ordos Basin," *China Petroleum Exploration*, vol. 25, no. 3, pp. 146–155, 2020.
- [11] J. Duan, *Characteristics of Carbonate Reservoir in the Lower Paleozoic in the Southern Margin of Ordos Basin*, [M.S. thesis], Chengdu University of Technology, 2009.
- [12] Z. L. Wang, L. Wei, X. Z. Wang et al., "The process and mechanism of natural gas accumulation of Lower Paleozoic in Yan'an area Ordos Basin," *Acta Petrolei Sinica*, vol. 37, no. 1, pp. 99–110, 2016.
- [13] J. H. Wang, *Study on the Lower Paleozoic Reservoir Formation in the Southern Margin of Ordos Basin*, [M.S. thesis], Chengdu University of Technology, 2009.
- [14] C. G. Wang, Y. Wang, H. Z. Xu, Y. P. Sun, W. L. Yang, and T. H. Wu, "The characteristics of hydrocarbon accumulation and evolution of Lower Paleozoic source rocks in Ordos Basin," *Acta Petrolei Sinica*, vol. 30, no. 1, pp. 38–50, 2009.
- [15] Y. Li, A. P. Fan, R. C. Yang, Y. P. Sun, and N. Lenhardt, "Sedimentary facies control on sandstone reservoir properties: a case study from the permian shanxi formation in the southern ordos basin, central China," *Marine and Petroleum Geology*, vol. 129, pp. 1–16, 2021.
- [16] W. X. Han, S. Z. Tao, W. J. Ma, Y. Li, and G. X. Ou, "Reasons for carbon isotope rollover in the Yan'an gas field of the southern Ordos Basin, China: evidence from the geochemical comparison of gas from fluid inclusions with wells," *International Journal of Coal Geology*, vol. 234, pp. 1–11, 2021.
- [17] C. Y. Wang, Z. C. Wang, J. L. Wang, Y. Bao, and X. M. Hu, "Reconstruction of paleo river systems and distribution of sedimentary facies of Shanxi and lower Shihezi formations in southern Ordos Basin," *Journal of China University of Mining and Technology*, vol. 18, no. 2, pp. 241–244, 2008.
- [18] Z. X. An, "The formation of northern Shaanxi gas area and the central paleo-uplift, China Offshore Oil and Gas," vol. 12, no. 3, pp. 150–153, 1998.
- [19] H. J. Gan, J. K. Mi, and X. M. Xiao, "Research on natural gas source and migration and accumulation of the gas field in the Upper Paleozoic in the north-central Ordos Basin," *Journal of Oil and Gas Technology*, vol. 29, no. 1, pp. 16–22, 2007.
- [20] L. Zhao, X. X. Xia, and J. X. Dai, "Migration and accumulation of natural gas in the Upper Paleozoic in the Ordos Basin," *Earth and Environment*, vol. 28, no. 3, pp. 48–53, 2000.
- [21] S. Wang, "Ordos Basin superposed evolution and structural controls of coal forming activities," *Earth Science Frontiers*, vol. 24, no. 2, pp. 54–63, 2017.
- [22] Y. Yao, D. Liu, and T. Yan, "Geological and hydrogeological controls on the accumulation of coalbed methane in the Wei-bei field, southeastern Ordos Basin," *International Journal of Coal Geology*, vol. 121, pp. 148–159, 2014.
- [23] C. Guo, Y. C. Xia, D. M. Ma et al., "Geological conditions of coalbed methane accumulation in the Hancheng area, southeastern Ordos Basin, China: implications for coalbed methane high-yield potential," *Energy Exploration and Exploitation*, vol. 37, no. 3, pp. 922–944, 2019.
- [24] Z. X. He, *Evolution and Oil Gas of the Ordos Basin*, Petroleum Industry Press, Beijing, China, 2003.
- [25] H. Zhang, Z. P. Meng, and Z. L. He, "Study on the tectonic stress fields in the Ordos Coal Basin," *Journal of China Coal Society*, vol. 25, pp. 1–5, 2000.
- [26] Y. K. Zhang, L. F. Zhou, B. Dang, and W. Sun, "Relationship between the Mesozoic and Cenozoic tectonic stress fields and the hydrocarbon accumulation in the Ordos Basin," *Petroleum Geology & Experiment*, vol. 28, no. 3, pp. 215–219, 2006a.
- [27] L. L. Wang, B. Jiang, J. L. Wang, Z. H. Qu, and R. Chen, "Structural controls on joint development in the southeastern margin of the Ordos Basin," *Arabian Journal of Geosciences*, vol. 9, no. 5, p. 352, 2016.
- [28] H. Xu, D. Z. Tang, J. L. Zhao, S. Tao, S. Li, and Y. Fang, "Geologic controls of the production of coalbed methane in the Hancheng area, southeastern Ordos Basin," *Journal of Natural Gas Science and Engineering*, vol. 26, no. 26, pp. 156–162, 2015.
- [29] J. L. Liu, K. Y. Liu, and L. L. Gui, "Characteristics of fluid inclusions and hydrocarbon charging history of the Upper Paleozoic in the central Ordos Basin," *Journal of China University of Petroleum*, vol. 43, no. 2, pp. 13–25, 2019.
- [30] T. Lei, H. C. Deng, D. Wu et al., "Depositional model of the lower-middle Ordovician Majiagou Formation in Daniudi Gas Field, Ordos Basin," *Journal of Palaeogeography*, vol. 22, no. 3, pp. 523–538, 2020.

- [31] J. L. Liu, K. Y. Liu, and X. Huang, "Effect of sedimentary heterogeneities on hydrocarbon accumulations in the Permian Shanxi Formation, Ordos Basin, China: insight from an integrated stratigraphic forward and petroleum system modelling," *Marine and Petroleum Geology*, vol. 76, pp. 412–431, 2016.
- [32] J. Yang and X. Pei, *Geology of Natural Gas in China, v. 4(Ordos Basin)*, Petroleum Industry Press (in Chinese), 1996.
- [33] Y. Yang, W. Li, and L. Ma, "Tectonic and stratigraphic controls of hydrocarbon systems in the Ordos Basin: a multicycle cratonic basin in central China," *AAPG Bulletin*, vol. 89, no. 2, pp. 255–269, 2005.
- [34] W. Z. Zhang, H. Yang, C. L. Zan, and Q. F. Kong, "Study on the geochemistry of natural gas in Paleozoic in the high thermal evolution area located the central - southern Yishan Slope, Ordos Basin," *Geochimica*, vol. 45, no. 6, pp. 614–622, 2016.
- [35] D. Middleton, J. Parnell, P. Carey, and G. Xu, "Reconstruction of fluid migration history of Northwest Ireland using fluid inclusion studies," *Journal of Geochemical Exploration*, no. 69, pp. 633–677, 2000.
- [36] J. Li, J. Z. Zhao, D. X. Wang et al., "Origin and source of natural gas in the Ordovician middle assemblage on the east side of the central paleo-uplift of the Ordos Basin," *Acta Petrolei Sinica*, vol. 37, no. 7, pp. 821–831, 2016.
- [37] X. Sun, J. Wang, C. Tao et al., "Geochemical characteristics and source of Paleozoic natural gas in Daniudi, Ordos Basin," *Acta Petrolei Sinica*, vol. 43, no. 2, pp. 307–314, 2021.
- [38] J. Q. Tu, Y. G. Dong, B. Z. Zhang et al., "Discovery of large-scale effective source rocks of Ordovician Majiagou Formation in Ordos Basin and its geological significance," *Natural Gas Industry*, vol. 36, no. 5, pp. 15–24, 2016.
- [39] J. X. Dai, X. Y. Xia, S. F. Qin, and J. Z. Zhao, "Causes of carbon isotope series reverse of organic alkane gas in China," *Oil & Gas Geology*, vol. 24, no. 1, pp. 1–6, 2003.
- [40] M. Schoell, "Genetic characterization of natural gases," *AAPG Bulletin*, vol. 67, no. 12, pp. 2225–2238, 1983.
- [41] L. Li, H. M. Tang, X. Wang et al., "Evolution of diagenetic fluid of ultra-deep Cretaceous Bashijiqike Formation in Kuqa depression," *Journal of Central South University*, vol. 25, no. 10, pp. 2472–2495, 2018.
- [42] J. Kelly, J. Parnell, and H. C. Chen, "Application of fluid inclusions to studies of fractured sandstone reservoirs," *Journal of Geochemical Exploration*, vol. 69–70, pp. 705–709, 2000.
- [43] A. M. Ingrid, "Petroleum inclusions in sedimentary basins: systematics, analytical methods and applications," *Lithos*, vol. 55, no. 1–4, pp. 195–212, 2001.
- [44] Q. Cao, J. Z. Zhao, J. H. Fu et al., "Gas source conditions of quasi-continuous gas reservoirs in the Upper Paleozoic of Ordos Basin," *Oil & Gas Geology*, vol. 34, no. 5, pp. 584–591, 2013.
- [45] J. H. Fu, X. S. Wei, S. S. Luo et al., "Discovery and geological understanding of Qingyang deep coal-derived gas field," *Petroleum Exploration and Development*, vol. 46, no. 6, pp. 1047–1061, 2019.
- [46] J. Z. Zhao, "Analysis of application examples of oil and gas inclusions in the study of accumulation chronology," *Earth and Environment*, vol. 30, no. 2, pp. 83–89, 2002.
- [47] X. M. Xiao, Z. F. Liu, and D. H. Liu, "Using reservoir fluid inclusion information to study the accumulation time of natural gas reservoirs," *Chinese Science Bulletin*, vol. 47, no. 12, pp. 957–960, 2002.
- [48] D. L. Liu, S. Z. Tao, and B. M. Zhang, "Application of inclusions in determining the age of accumulation and problems needing attention," *Natural Gas Geoscience*, vol. 16, no. 1, pp. 16–19, 2005.
- [49] R. X. Li, S. L. Xi, and L. J. Di, "Using reservoir oil and gas inclusion petrography to determine the period of oil and gas accumulation-taking Longdong oilfield in Ordos Basin as an example," *Oil & Gas Geology*, vol. 27, no. 2, pp. 194–199, 2006.
- [50] Z. L. Ren, S. Zhang, S. L. Gao, J. P. Cui, Y. Y. Xiao, and H. Xiao, "The tectonic thermal evolution history of Ordos Basin and its significance of accumulation and mineralization," *Scientia Sinica (Terrae)*, vol. 37, no. S1, pp. 23–32, 2007.